Deep Trench Capacitor Drive of a 3.3 GHz Unreleased Si MEMS Resonator

Wentao Wang and Dana Weinstein

HybridMEMS Lab, Massachusetts Institute of Technology
77 Massachusetts Ave, Cambridge, MA, USA
Email: wangwt@mit.edu

Abstract

This work presents unreleased RF bulk acoustic resonators using Deep Trench (DT) capacitors for both transduction and acoustic isolation. While the majority of Si MEMS resonators require a release step to freely suspend the resonant cavity, these unreleased resonators are formed entirely in solid media. This eliminates the need for complex release steps and costly packaging. The resonators use 1D periodic DT structures etched into a bulk Si substrate for both electrostatic transduction and to form Acoustic Bragg Reflectors (ABRs) for energy localization. In this paper, we introduce the concept of Deep Trenches as ABRs, and provide analysis, simulation, and experimental verification of their use for high-Q resonators. A 3.3 GHz unreleased Si resonator is demonstrated with Q of 2057 and motional impedance R_X of 1.2 kΩ. This realization of high-Q unreleased resonators in a bulk Si process provides a high yield, low cost, no packaging solution for on-chip clocking, wireless communication, and electromechanical signal processing.

Introduction

With frequency-quality factor products ($f{\cdot}Q$) often exceeding 10^{13}, micro-electomechanical resonators offer a high-Q, small footprint alternative to conventional LC tanks and off-chip crystals for clocking and wireless communication. Over the past three decades, much progress has been made in the key figures of merit of MEMS resonators including small footprint, high Q, low motional impedance, efficient energy coupling k_T^2. In parallel, efforts have focused on system-level metrics including high yield, low cost, robustness, easy packaging and integration with circuits. One of the key challenges in MEMS resonator design is to achieve high performance yet manufacturable devices. The unreleased Deep Trench (DT) resonators in this work address this challenge.

Beyond the performance goals of high Q and low loss, these devices target two key features desired for monolithically integrated MEMS resonators. First, lithographic definition of resonance frequency enables a broad range of frequencies to be fabricated on a single chip. Second, unreleased bulk-acoustic resonators do not require any low-yield, complex steps to freely suspend the moving structure, and are robust in harsh environments without packaging. Unreleased resonators such as the HBAR (1), launching acoustic waves into a solid device, have been demonstrated but have thickness-defined frequency. Lateral bulk acoustic resonators with lithographically defined frequency such as the LoBAR (2) have achieved high Q, but require low d_{31} coupling to drive and sense resonance.

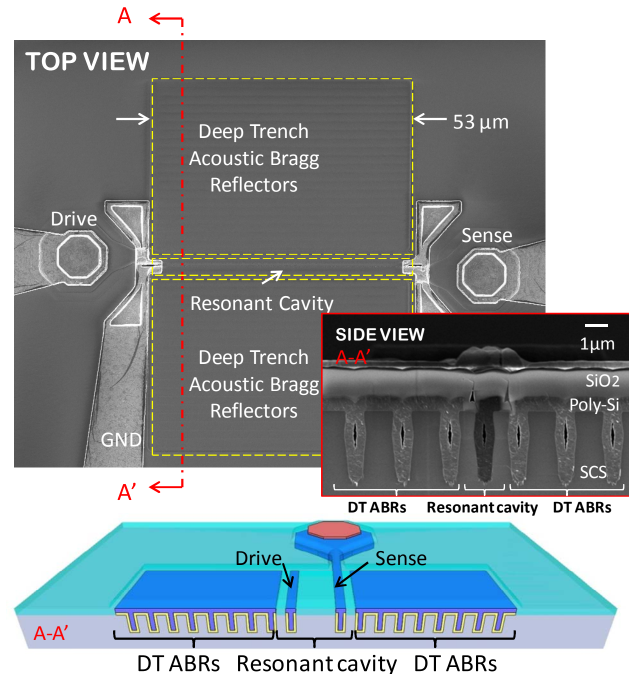

Fig. 1. Scanning electron micrographs (top) and schematic (bottom) of unreleased Deep Trench (DT) MEMS resonator. Acoustic Bragg reflectors (ABRs) formed from periodically spaced DTs define a high-Q resonant cavity in the center of the device. DT capacitors inside the resonant cavity form electrostatic drive and sense transducers.

Meanwhile, sidewall AlN resonators (3) excite lateral resonance with d_{33} coupling, but still require a release step. The unreleased Si DT resonators introduced in this work provide the benefits of all of these devices with high Q, efficient dielectric transduction, lateral resonance, and no release step. The DT resonator implements Deep Trench capacitors as both electrostatic transducers and Acoustic Bragg Reflectors (ABRs), defined in a single mask (Fig. 1). While ABRs provide acoustic isolation in a solid medium, the DT capacitors function as Internal Dielectric Transducers (4), which have achieved the highest frequencies and among the highest $f{\cdot}Q$ products in Si to date (5-6).

Deep Trench Resonator Design

A. Theory of DT Acoustic Bragg Reflectors and Resonators

The ABR utilizes two alternating materials of high and low acoustic impedance to provide high acoustic reflection at the boundaries of the resonator. The resonance cavity of the DT resonator is formed in the plane of the wafer so that the resonance frequency can be lithographically defined. In this work, material pairs of Single-Crystal Silicon (SCS) and Polycrystalline Silicon (PolySi) are used to form DT ABRs.

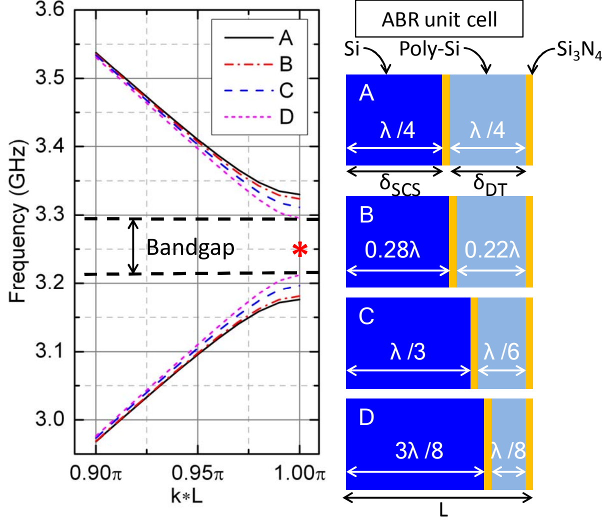

Fig. 2. Simulated band structure of DT ABRs formed by alternating layers of SCS and PolySi. Unit cells of 4 different DT ABRs are shown with various ratios of SCS and PolySi. This ratio determines the width of the bandgap generated by the ABR. Bandgap center is aligned by keeping the cell length at λ/2. Design B corresponds to the design experimentally demonstrated in this paper.

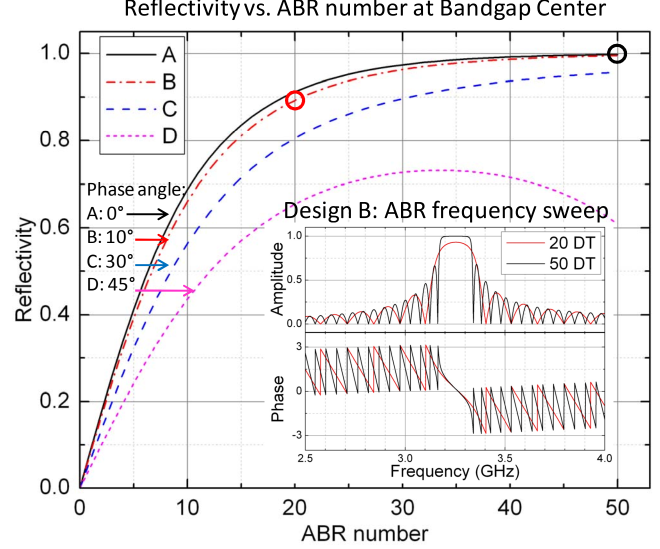

Fig. 3. Reflectivity of DT ABRs as a function of ABR pair number plotted at the ∗ position in Fig. 2. The more δ_{DT} and δ_{SCS} deviate from λ/4, the larger the phase shift of reflectivity.

An acoustic impedance ratio of $Z_{SCS}/Z_{Poly} = 1.09$ is assumed (7). While this ratio of acoustic impedance is low compared to other conventional materials, this material choice is motivated by low loss mechanical properties of Si and the similarity to DRAM DT capacitors (8).

In the case of released resonators, eigenmodes can be calculated readily using the free boundary conditions at edges of the resonator body. For the unreleased resonators, complexity arises in that the ABR boundary may induce phase change, and its reflectivity is a function of frequency. This prevents an obvious eigenmode decomposition inside the resonator; although the reflectivity amplitude converges to 1 as the number of ABR layers increase, it cannot be treated as a free surface. In this study, two methods are used to analyze the unreleased resonator bounded with ABRs:

1. The ABR is treated numerically by wave superposition to find out the complex reflectivity value, which is used for resonator eigenmode calculation (9).
2. The eigenmode of the resonator-ABR composite structure is directly calculated through finite element simulation in COMSOL using Perfectly Matched Layers (PML).

Typically, ABRs are designed with alternating materials at quarter wavelength of the targeted reflector frequency, and the resonant cavity is at integer multiples of half-wavelengths (9-10) (e.g. Fig. 2, Design A). This design provides optimal performance and zero phase change as seen at the resonator-ABR interface. However, for a DT resonator the priority in design is effective fabrication, i.e. fixing the trench length δ_{DT} for uniform etch rates and optimal trench fill. Consequently, the only design parameter is the spacing between DTs for modification of the reflective frequency. With this design, both high and low acoustic impedance layers will deviate from quarter wavelength, resulting in a narrowing of DT ABR bandgap (Fig. 2) and degradation of reflectivity (Fig. 3). The capacitor dielectric, in this case 15nm of Si_3N_4 (shown in yellow in Fig. 2), is sandwiched between the bulk SCS and PolySi trench fill. This does not affect band structure and reflectivity analysis of the ABR as long as the dielectric's fractional wavelength is much smaller than that in the other two materials.

The bandgaps and reflectivity of the DT ABR can be calculated numerically from the recursion expressions:

$$R_1(n) = r_{12} + \frac{t_{12}t_{21}R_2(n)e^{-i2\delta_2}}{1 - r_{21}R_2(n)e^{-i2\delta_2}} \quad (1)$$

$$R_2(n) = r_{21} + \frac{t_{12}t_{21}R_1(n-1)e^{-i2\delta_1}}{1 - r_{12}R_1(n-1)e^{-i2\delta_1}} \quad (2)$$

in which SCS and PolySi are designated as materials 1 and 2. r_{ij} and t_{ij} represent the reflection and transmission coefficients from medium *i* to *j*, *n* is the layer number, and δ_i is the thickness of medium *i*.

Fig. 3 illustrates the dependence of the reflectivity amplitude on the number of ABRs for each of the 4 designs in Fig. 2: Designs A—D. It can be observed that the narrower the bandgap, the slower the convergence of reflectivity to 1. The inset of Fig. 3 shows the frequency dependence of reflectivity of Design B for 20 DTs and 50 DTs. Perfect reflectivity only exists inside the bandgap, and zero phase shift only exists at the bandgap center. Furthermore, as the DT lengths and spacings deviate from λ/4 (Design B—D), a non-zero phase of reflectivity is introduced at the resonator-ABR interface. This phase implies that the standing wave inside the resonant cavity is no longer an integer multiple of half-wavelength, but is rather controlled by a combination of the cavity length and the ABR reflectivity phase.

B. Design Rules of DT Resonators

This new phenomenon makes the DT resonator design challenging: frequency cannot be calculated from the "as-

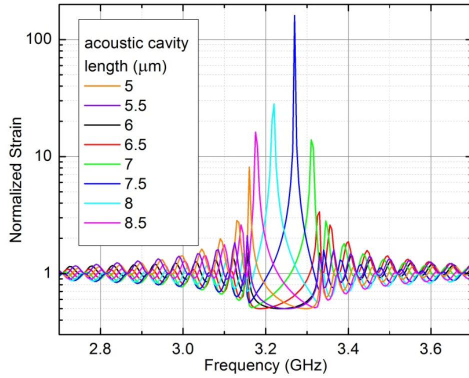

Fig. 4. Simulated frequency response of varying acoustic cavity lengths with 50 fixed DT ABRs (Design B: 950nm trench length δ_{DT}, with $\delta_{DT} + \delta_{SCS} = 1.7\mu m$ pitch). Strain is normalized to strain induced at the transducer.

seen" cavity length. A better approach is work backwards—instead of designing resonators and matching boundaries, one can design boundaries and match the resonant cavity.

1. DT length δ_{DT} is selected based on optimum process parameters for trench etch and fill.
2. DT spacing δ_{SCS} is chosen according to the targeted resonator frequency by numerical calculation. The DT ABR determines the frequency range where high-Q resonance can be sustained.
3. With fixed DT length and spacing, the cavity length is varied to find the resonance inside the bandgap (Fig. 4).

To maximize Q and mode uniformity, the dimension perpendicular to the longitudinal resonance must be designed for minimum acoustic reflections. A thick capping material matched acoustically to the resonator material should be used to reduce spurious modes and ensure mode uniformity. In Fig. 5, COMSOL simulation verifies that a good acoustic impedance match in the direction perpendicular to resonance enhances Q. PolySi and SiO_2 cap the top of the resonator in this design.

C. DT Electrostatic Transducer

As previously mentioned, DT capacitors identical to the ABR DTs are used as drive and sense transducers inside the resonator. The authors have previously demonstrated this Internal Dielectric Transduction in released resonators, achieving the highest frequencies and among the highest $f{\cdot}Q$ products in passive Si devices to date (6). Unlike any other transducer, this dielectric transduction improves in efficiency as resonator frequency increases, and is ideal for the multi-GHz domain. It should be noted that each DT capacitor is composed of two internal dielectric transducers, which doubles the transducer area, as long as $\delta_{DT} \ll \lambda/2$.

Fabrication

The resonators were fabricated at MIT's Microsystems Technology Laboratory (MTL) in bulk Silicon, as detailed in Fig. 6. (a) A low resistivity bulk Si wafer patterned with a hard mask to define 4.5μm Deep Trenches (DTs) in Cl_2/HBr ICP RIE. (b)The trenches are lined with 15nm Si_3N_4 and filled with n-type doped polysilicon. (c) The PolySi is patterned for electrical isolation of the transducer and to make contact to the substrate. The unreleased resonators are then capped with 1.5 μm field oxide (FOX) to ensure 3D confinement of the resonant cavity and to reduce pad and routing parasitics. (d) The FOX is patterned for metal contact to the transducer DT and substrate. Finally, a TiN/Al metal layer is sputtered, patterned by Cl_2/BCl_3 RIE, and sintered at 450°C in H_2/N_2 gases. It should be noted that Si_3N_4 lines the trenches to form the transduction capacitors, but its acoustic effect is negligible since the wavelength at operating frequency is far larger than the film thickness.

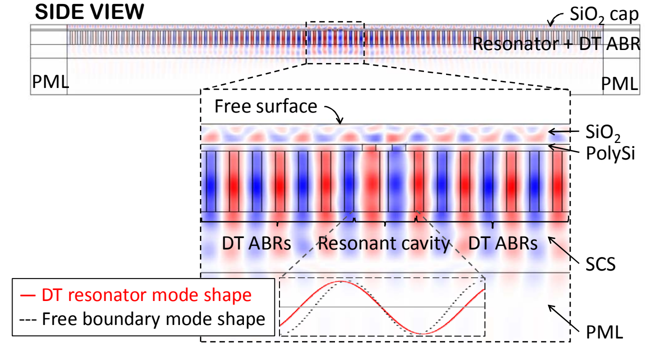

Fig. 5. COMSOL simulation of an unreleased DT resonator where drive DT is centered in the resonant cavity. Red and blue indicate peak and trough of displacement in the x direction. The inset shows the influence of non-zero phase at the resonator-ABR interface on the resonance mode.

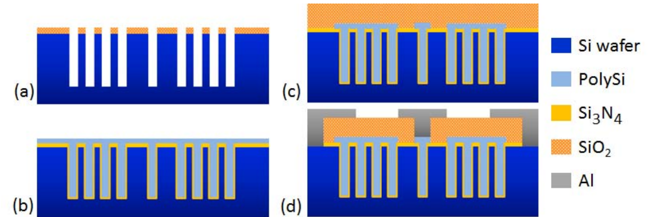

Fig. 6. Fabrication process of unreleased DT resonators similar to that used for DRAM capacitors.

Experimental Setup and Results

Devices were tested in air at room temperature in an RF probe station using a pseudo-differential measurement as shown in Fig. 7 to cancel parasitic capacitance of both pads (C_{pad}=300 fF) and device (C_0=440 fF). No on-chip de-embedding is performed.

The frequency response of two unreleased DT resonators is shown in Fig. 8. Since zero bias voltage is applied across the transducers of the dummy resonator, it does not contribute to the differential output SDD21. Therefore, the resonator's motional impedance $R_x \equiv v_{in}/i_{out}$ can be extracted directly from SDD21 as $SDD21(dB) = 20\log\left(Z_0/(R_x + Z_0)\right)$ (12).

Applying an RF signal of -5 dBm and varying DC bias on the input and output transducers, the devices show clear resonance at 3.2 GHz for a device with 20 ABRs, and 3.3 GHz for a device with 50 ABRs. Wide frequency sweeps showed no spurious modes in the multi-GHz range around resonance. The 50 ABR resonator exhibits a Q of 2057 and R_x of 1.2 kΩ. This translates to an $f{\cdot}Q$ product of 6.8×10^{12}, and k_T^2 of 5.4×10^{-5}. This coupling coefficient can be

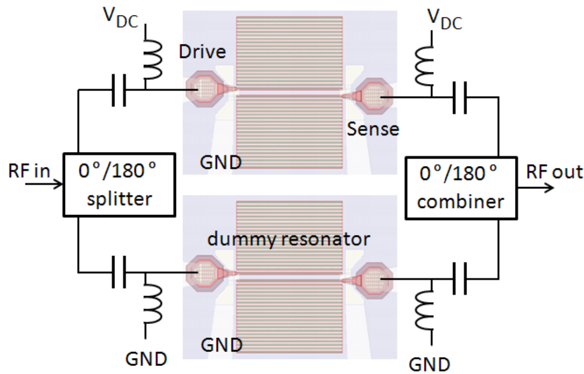

Fig. 7. Measurement setup for pseudo-differential testing of DT resonator. An identical dummy resonator which is not driven (no DC voltage applied) provides differential cancelation of the pad and device capacitance.

dramatically improved by scaling the dielectric.

As expected, the 50 ABR resonator shows improved performance of both Q and R_x relative to the 20 ABR resonator. This result is in agreement with the theory of DT bandgaps, which predicts ~10% improvement in ABR reflectivity between 20 and 50 ABRs (Fig. 3). An identical resonator with only 1 ABR exhibited no measurable resonance.

In addition, this experimental result shows good

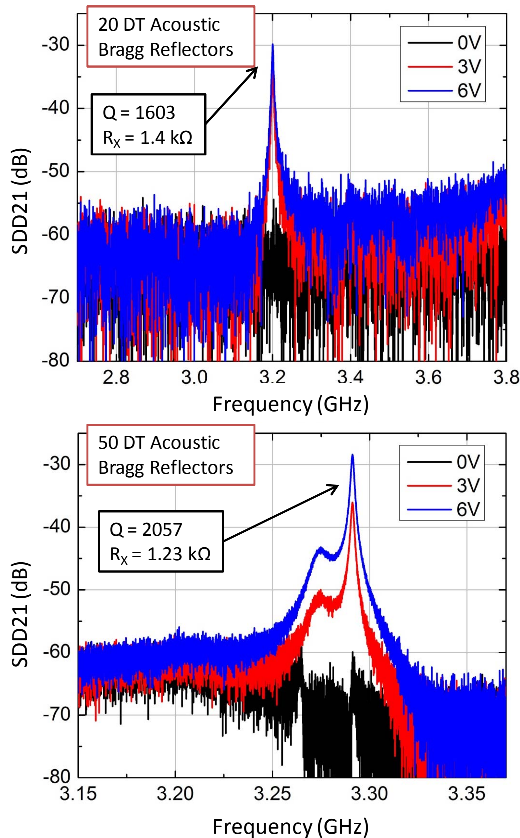

Fig. 8. Measured frequency response of DT resonators with 7.2 µm long resonant cavity, DT length of 950nm, and 1.7µm DT pitch in the ABRs. Devices with 20 ABRs and 50 ABRs are shown, with higher Q and lower loss in the latter. Wide frequency sweeps show no spurious modes in a multi-GHz range.

agreement with numerical analysis (Fig. 4). The 0.1 GHz frequency shift with the increase of ABR number is caused by the phase change of reflectivity as the ABR number increases. This frequency shift from an increased ABR number is also observed in COMSOL simulation.

Conclusion

A 3.3 GHz unreleased resonator with Deep Trench dielectric drive and sense was demonstrated with performance rivaling that of freely-suspended Si resonators in the same frequency range. Deep Trenches were implemented both as electrostatic transducers and as Acoustic Bragg Reflectors to localize vibrations in the unreleased resonator. This new concept enables high Q, low loss multi-GHz resonators in a simple, robust manufacturing process.

The authors recently demonstrated the first unreleased MEMS resonators in IBM's 32nm SOI process, with no need for post-processing or packaging (11). Resonators were realized at the transistor level, driven with gate dielectric capacitors, and acoustically defined with ABRs formed with Shallow Trench Isolation (STI). Deep Trenches available in the IBM 32nm and 45nm SOI for DRAM (8) provide vertical capacitors similar to those in (4) and can form Bragg reflectors with much higher aspect ratios than (11). This first demonstration of DT resonators in Silicon paves the way for high-Q multi-GHz frequency sources intimately integrated in CMOS with no post-processing.

References

(1) J.T. Haynes, M.S. Buchalter, R.A. Moore, H.L. Salvo, S.G. Shepherd, B.R. McAvoy, "Stable microwave source using high overtone bulk resonators," *IEEE MTT-S* 1985, pp. 243-246.
(2) M. Ziaei-Moayyed, S.D. Habermehl, D.W. Branch, P.J. Clews, R.H. Olsson III, "Silicon carbide lateral overtone Bulk Acoustic Resonator with ultrahigh quality factor," *IEEE MEMS*, 2011, pp. 788-792.
(3) R. Tabrizian, F. Ayazi, "Laterally excited silicon Bulk Acoustic Resonator with sidewall AlN," *Int. Conf. on Solid-State Sensors, Acutators and Microsystems (Transducers),* 2011, pp. 1520-1523.
(4) D. Weinstein, S.A. Bhave, "Internal dielectric transduction of a 4.5 GHz silicon bar resonator," *IEEE Int. Elec. Dev. Meeting (IEDM),* 2007, pp. 415-418.
(5) W. Wang, L.C. Popa, R. Marathe, D. Weinstein, "An unreleased mm-wave resonant body transistor," *IEEE MEMS,* 2011, pp. 1341-1344.
(6) D. Weinstein, S.A. Bhave, "Internal dielectric transduction in bulk-mode resonators," *IEEE Journal of Microelectromechanical Systems (JMEMS)*, 18(6), 2009, pp.1401-1408.
(7) W.N. Sharpe, Jr.B. Yuan, R. Vaidyanathan, "Measurements of Young's modulus, Poisson's ratio, and tensile strength of polysilicon," *IEEE MEMS,* 1997, pp. 424-429.
(8) G. Wang et al, "Scaling deep trench based eDRAM on SOI to 32nm and beyond," *IEEE Int. Elec. Dev. Meeting (IEDM),* 2009, pp. 11.1.1-11.1.4.
(9) W. Wang, D. Weinstein, "Acoustic Bragg reflectors for *Q*-enhancement of unreleased MEMS resonators," *IEEE Frequency Control Symposium (FCS)*, 2011, pp. 759-764.
(10) K.M. Lakin, K.T. McCarron, R.E. Rose, "Solidly Mounted Resonators and Filters," *IEEE Ultrasonics Symposium*, 1995, pp. 905-908.
(11) R. Marathe, W. Wang, D. Weinstein, "Si-based unreleased hybrid MEMS-CMOS resonators in 32nm technology," *IEEE MEMS*, 2012, pp. 729-732.
(12) P. Rantakari, J. Kiihamäki, M. Koskenvuori, T. Lamminmäki, I. Tittonen, "Reducing the effect of parasitic capacitance on MEMS measurements," *Int. Conf. on Solid-State Sensors, Acutators and Microsystems (Transducers),* 2001, pp. 1556-1559.